Competing strain effects in reactivity of $LaCoO_3$ with oxygen

Akihiro Kushima,[1] Sidney Yip,[1,2] and Bilge Yildiz[1,*]
[1]*Department of Nuclear Science and Engineering, Massachusetts Institute of Technology, 77 Massachusetts Avenue, Cambridge, Massachusetts 02139, USA*
[2]*Department of Materials Science and Engineering, Massachusetts Institute of Technology, 77 Massachusetts Avenue, Cambridge, Massachusetts 02139, USA*
(Received 16 April 2010; revised manuscript received 5 August 2010; published 17 September 2010)

Planar strain effects on oxygen-vacancy formation and oxygen adsorption on $LaCoO_3$ are shown to manifest through competing mechanisms. Through first-principles calculations, we demonstrate that these unit processes are facilitated by elastic stretching. On the other hand, spin-state transitions and Co-O bond exchange hinder these processes by trapping the lattice oxygen with increasing tensile strain. A transition from chemisorption to physisorption of the oxygen molecule is identified at high strains. Insights on charge-density profiles, density of electronic states, and stress thresholds suggest the possibility of tuning strain-mediated reactivity in $LaCoO_3$ and related perovskite oxides.

DOI: 10.1103/PhysRevB.82.115435 PACS number(s): 62.20.−x, 31.15.ae, 82.45.Jn

I. INTRODUCTION

External electromagnetic fields or mechanical strains give rise to unusual electronic and magnetic state transitions in a number of 3*d* transition-metal (TM) oxides, such as the $La_{1-x}Sr_xMnO_3$ (LSM) (Ref. 1) and $La_{1-x}Sr_xCoO_3$ (LSC) (Ref. 2) families of perovskite compounds. In particular, LSC exhibits notable strain effects on its electrical transport and magnetic state.[3–5] LSM and LSC also have been treated as model catalysts and mixed ionic and electronic conductors for high-temperature applications that involve oxygen reactions.[6] In enabling fast oxygen reduction and transport through these materials, their surface and bulk reactivities play important roles. First-principles and atomistic calculations[7–9] have shown the unit processes governing oxygen reduction to consist of oxygen molecule adsorption followed by dissociation into a neighboring oxygen vacancy and transport into the bulk through a vacancy-mediated mechanism. Thus, both the adsorption process and the equilibrium vacancy concentrations contribute to the TM oxide reactivity. While the underlying strain effects were shown to alter the stable oxygen-vacancy configurations in some oxide systems,[10–12] systematic studies to clarify the competing microscopic mechanisms and the magnitude of these effects have not been carried out.

In this study, we determine the dominant strain-driven mechanisms governing oxygen-vacancy formation in the bulk, and oxygen molecular adsorption and vacancy formation on the surface of $LaCoO_3$ (LCO) by performing first-principles calculations. $LaCoO_3$ was chosen as a model system with no ionic or electronic defects. We treat these unit processes separately from each other, solely to probe the mechanistic effects of strain on them. Mavrikakis *et al.* showed that the surface reactivity of the metal increases with biaxial lattice expansion, following a concurrent upshift of the metal *d* state.[13] For the TM perovskite, we find the picture is more complex. We identify the primary competing processes to be elastic stretching of the Co-O bonds which reduces the overlap of the Co *d* and O *p* bands, anisotropic local relaxations which break and reform the Co-O bonds, and phase transitions in spin state. The first two mechanisms are elastoplastic in nature while the third is magnetoelastic. We show that the elastoplastic effects cause a transition in the adsorption mechanism from chemisorption to physisorption. The magnetoelastic coupling introduces an additional degree of freedom, with the Co^{3+} d^6 ion displaying various spin states due to a delicate balance between the crystal-field splitting and the intra-atomic Hund's exchange.[14] Variations in the Co-O bond length, the Co-O-Co angle, and the tilt pattern of the CoO_6 octahedra are known to be important in the magnetic and electronic-structure transitions in the strain-induced pseudotetragonal LCO.[3,4] These in turn give rise to electron localization and Co-O bond strength alterations which are also important in the LCO reactivity.

An implication of this work is the prospect of controlling the TM oxide reactivity through strain to develop highly active ionic nanostructures in, for example, solid oxide fuel cells, sensors, and batteries. Nanoscale heterointerfaces which can introduce large coherent strains are a promising direction for this purpose.[15,16] The examples to date include strained yttria stabilized zirconia (YSZ) (Refs. 17–19) and heterointerface of $(La,Sr)_2CoO_4/(La,Sr)CoO_3$ (Ref. 20) thin films. These structures have been shown to exhibit several orders of magnitude higher ionic conductivity and oxygen exchange rate compared to their unstrained single-phase states. The mechanistic insights discussed here concerning strain-induced bulk and surface reactivities are not limited only to oxygen in LCO, they can be extended to other ionic TM oxides. Additionally, probing the strain response of the oxygen defects in the LSC family can give insights to the indirect chemical effects of strain on magnetic state transition mechanisms.[21]

II. SIMULATION APPROACH

We applied density-functional theory (DFT) formalism in the generalized gradient approximation parameterized by Perdew and Wang[22] using plane-wave basis set to calculate the energetics described in this paper. To avoid the self-interaction errors that occur in the traditional DFT for

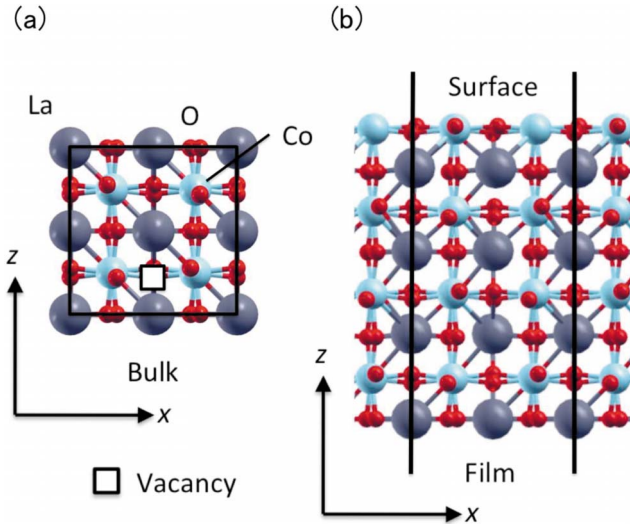

FIG. 1. (Color online) Simulation models of the $LaCoO_3$ (a) bulk, and (b) surface calculations. Large gray, light blue, and small red (large dark, light, and small dark in print) spheres indicate La, Co, and O atoms, respectively. Solid lines in the figure indicate the simulation cell.

strongly correlated electronic systems, we employed the DFT+U method accounting for the on-site Coulomb interaction in the localized d or f orbitals.[23] The correction parameter of effective $U-J=3.3$ eV was chosen, as determined in Ref. 24 by fitting the enthalpies of oxidation reactions. The ionic cores were represented with projector-augmented wave potentials[25] as implemented in the Vienna *ab initio* simulation package (VASP).[26] An energy cut off of 600 eV was chosen for expanding the wave functions. A $2\times2\times2$ Monkhorst-Pack k-point mesh[27] was used for a $2\times2\times2$ unit cell representing the bulk LCO, and a $2\times2\times1$ mesh was used for a slab of $2\times2\times4$ unit cells containing eight atomic layers with 1 nm of vacuum region in the z direction for the LCO surface calculations. The simulation models are shown in Fig. 1. The total energy of the system with respect to the k-point mesh and the energy cutoff for the system converged within 0.1%. The LCO unit cell contains one La, one Co, and three O atoms with a fully relaxed lattice constant of 3.83 Å and Co-O-Co angle of 162° in agreement with experimentally measured values.[3] Two-dimensional-planar lattice strain was imposed by elongating the simulation cell in the x and y directions and relaxing the cell configuration and dimension in the z direction. For the surface calculations, the atoms in the bottom two layers were fixed at the bulk coordinates and the rest of the atoms were allowed to relax.

The oxygen-vacancy formation energies in the bulk and surface, E_{vac}^{B} and E_{vac}^{S} serve as a measure of the strain response of oxygen defect chemistry. The low index (100) surface of LCO was used in assessing the two surface energies, oxygen-vacancy formation E_{vac}^{S} and adsorption energy, E_{ad}, which control the surface reactivity. Oxygen molecule in the tilted configuration[8] was considered here as the most stable adsorption configuration on the Co ion. $E_{vac}^{B,S}$ and E_{ad} were defined as,

$$E_{vac}^{B,S} = E_v - E_0 + 1/2E_{O_2}, \quad (1)$$

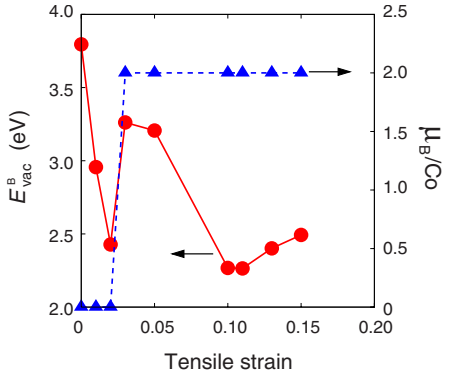

FIG. 2. (Color online) Vacancy formation energy E_{vac}^{B} (circles) and magnetization (triangles) as a function of lattice strain in the bulk $LaCoO_3$.

$$E_{ad} = E' - E_0 - E_{O_2}, \quad (2)$$

where E_v, E', E_0, and E_{O_2} are the system energies with one vacancy, adsorbed O_2, no vacancy or O_2, and an isolated O_2 molecule, respectively.

The maximum strain considered here was 15%. When a vacancy was introduced beyond 11% strain, the bulk cations were restrained to their perovskite positions. These very large strains cannot be supported by LCO films of tens or hundreds of nanometer thickness grown on a substrate.[28] We treat the structure and strain conditions here as an ideal defect-free system in probing the dominant mechanisms operating on the oxygen sublattice under strain. Real defected LCO structures may exhibit similar phenomenon as identified here, at smaller global strain states. Such large strain states could be achieved only locally, for example, in the vicinity of dopants of different radii[29] and extended defects.

III. RESULTS AND DISCUSSION

A. Bulk reactivity vs strain

We present first our results on bulk reactivity, namely, the vacancy formation energy, E_{vac}^{B} which determines the equilibrium anion vacancy concentration. Lower value of E_{vac}^{B} means vacancy formation is favored, which also enables more facile kinetics of incorporation of the adsorbed oxygen into the bulk and its ionic transport therein. Figure 2 shows the variations in E_{vac}^{B} and the magnetic moment, μ_B/Co, with tensile lattice strain in LCO. In the unstrained state, the LCO bulk is at the low-spin (LS) state. It is reasonable to expect that in general tensile strain, in the form of elastic stretching, will act to lower E_{vac}^{B} by weakening the Co-O bond, as is the case here up to $\varepsilon=0.02$ shown in Fig. 3. However, two significant reversals of this trend are seen, at $\varepsilon=0.03$ and again at $\varepsilon=0.11$. The first increase in E_{vac}^{B} is very well correlated with the jump in magnetic moment at $\varepsilon=0.03$. Thus, this reversal is attributed to a spin transition from the state LS, characterized by a cubiclike charge-density distribution around the Co ion,[30] to the intermediate-spin (IS) state with a spherical distribution and stronger Co-O overlap, as can be seen in Fig. 3. At the strain $\varepsilon=0.11$, where the second reversal occurs, we find the atomic configuration undergoes a lo-

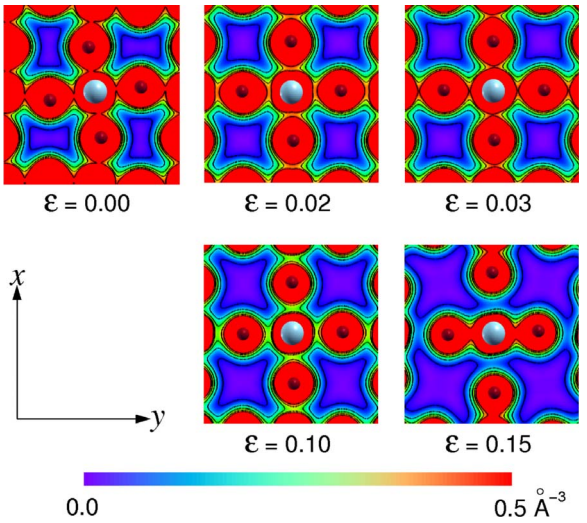

FIG. 3. (Color online) Electronic charge-density distribution of the valence electrons on the CoO_2 xy plane as a function of strain, ε, before the introduction of oxygen vacancy to the model. Large spheres are Co and small spheres are O atoms.

cal rebonding with rupture of two nearest-neighbor Co-O bonds in the xy plane and strengthening of the other two, again seen in Fig. 3. This configurational change results in the trapping of two oxygen ions for each Co and increase in E^{B}_{vac}. Our claims of bond strengthening and weakening induced by the magnetoelastic and elastoplastic transitions here are supported by our density of states (DOS) calculations showing the extent of the hybridization between the Co d bands and O p bands. Orbital projected DOS for Co d orbital and O p orbital at various strains are shown in Fig. 4. Overlapping of Co d orbital and O p orbital depicts the orbital hybridization and Co-O binding in the bulk of $LaCoO_3$. At $\varepsilon=0.00$, strong hybridization of the DOS peaks at −4 eV and −4.7 eV is evident. As lattice strain increases up to $\varepsilon=0.02$, the overlap of the peaks decrease, indicating the weakening of the Co-O bond during elastic stretching. This decrease in the hybridization driven by elastic stretching was reversed twice at larger strains. First at $\varepsilon=0.03$ where the spin state changes from LS to IS, the hybridization of the Co d orbital and O p orbital in DOS reemerges near −6 eV. At $0.03<\varepsilon<0.10$, the overlap in the DOS peaks decreases again due to the elastic stretching of the Co-O bonds in the IS state, corresponding to the second decrease in E^{B}_{vac}. Second, beyond $\varepsilon=0.10$, hybridization of the Co d orbital and O p orbital strengthens near −5 eV because of the strengthening of the Co-O bond, and increases the E^{B}_{vac}. O-cation bond strengthening and the trapping of oxygen due to local relaxations at high strain states has been demonstrated in YSZ under tensile planar strain,[18] consistent with our observations here for LCO, although in the present case the magnetoelastic coupling in the LCO bulk added an extra degree of complexity to the relationship between strain and vacancy formation energy.

B. Surface reactivity vs strain

Next, we probe surface reactivities through oxygen adsorption and vacancy formation energies, E_{ad} and E^{S}_{vac}. Their

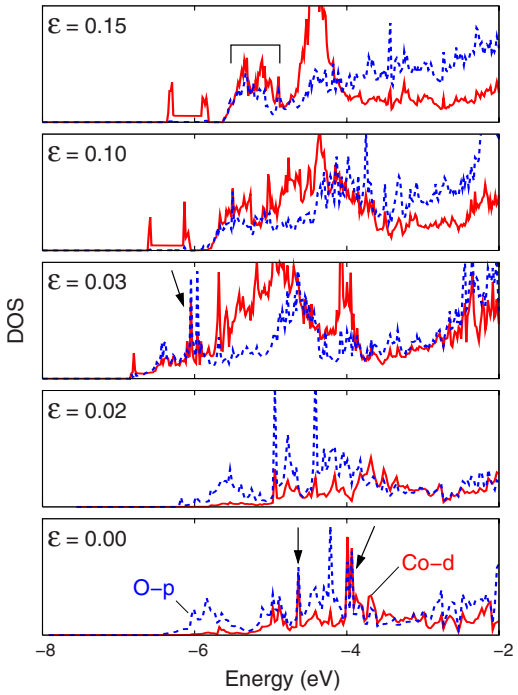

FIG. 4. (Color online) Orbital projected electronic density of states (DOS) for the Co d orbital and O p orbital with varying extent of hybridization at different strains in the bulk $LaCoO_3$ model. Arrows show the O p and Co d orbitals' hybridization.

variations with lattice strain are shown in Fig. 5. Unlike the LS state in the bulk, the LCO surface was in state IS at $\varepsilon=0.00$. We can again interpret the strain responses in terms of the charge-density distributions and local density of states both explicitly reported here. Compared to Fig. 2, Fig. 5 indicates only a single reversal of the tensile strain effect, at $\varepsilon=0.04$. Given the foregoing discussion on bulk reactivity, this is to be expected in the absence of a spin-state transition. For $\varepsilon>0.03$, we find significant strengthening of the Co-O bond due to local relaxations that trap oxygen, similar to that discussed above for bulk LCO at high strain.

The strain response of E_{ad} exhibits a similar trend as that of E^{S}_{vac}. At low strains, $\varepsilon\leq0.04$, the O_2 molecule chemisorbs on a Co ion, with its p orbital hybridizing with the Co d

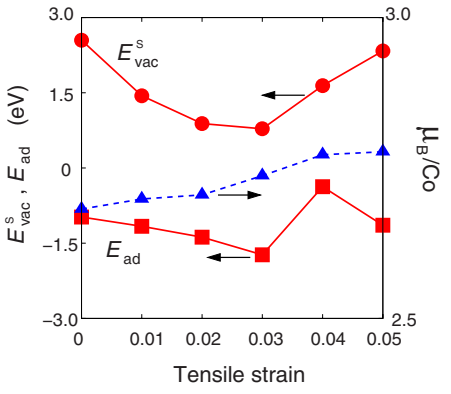

FIG. 5. (Color online) Vacancy formation energy E^{S}_{vac} (circles), oxygen adsorption energy E_{ad} (squares), and magnetization (triangles) on the $LaCoO_3$ surface as a function of lattice strain.

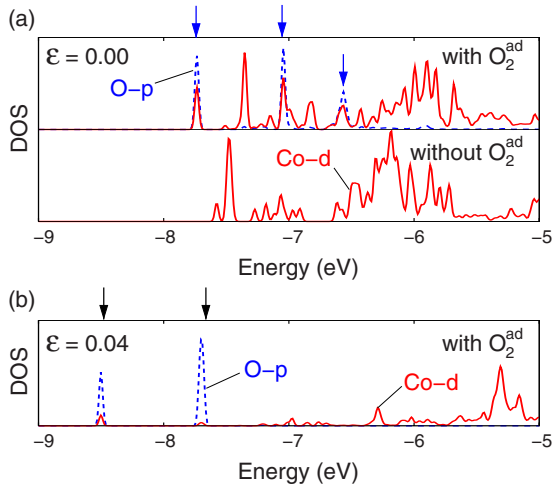

FIG. 6. (Color online) (a) At $\varepsilon=0.00$, Co d-orbital DOS only (lower panel) before oxygen adsorption (without O_2^{ad}), and Co d-orbital with the p-orbital DOS (upper panel) of adsorbed oxygen (with O_2^{ad}) on the $LaCoO_3$ surface after oxygen adsorption. (b) Co d orbital with the adsorbed oxygen p-orbital DOS on the $LaCoO_3$ surface at $\varepsilon=0.04$. Arrows show the adsorbed O p and surface Co d orbitals' hybridization.

orbital. This hybridization forms three prominently overlapped peaks, indicated by the arrows in Fig. 6(a)—upper panel. Furthermore, oxygen adsorption spreads and downshifts the Co d band. Here, the large change in Co d-band DOS after the adsorption implies the O_2 was chemisorbed to the surface Co.

Figure 7(a) shows that the Co d-band center on the $LaCoO_3$ surface without an adsorbed O_2 molecule increases monotonically with tensile strain. Reduction in E_{ad} with tensile strain due to the upshift of the d-orbital energy[13] and the reduction in coordination[31] was reported on transition-metal surfaces. This agrees with the decrease in E_{ad} in our calculations for $\varepsilon \leq 0.03$, corresponding to the upshift of the Co d band. We also consider the Co d-band center on the $LaCoO_3$ surface "with" an adsorbed O_2 molecule, which downshifts with strain as shown in Fig. 7(b). The downshift of this d-band energy from the bare state to the oxygen adsorption state is a measure of the relative relaxation of the system energy upon oxygen adsorption. The shift becomes more

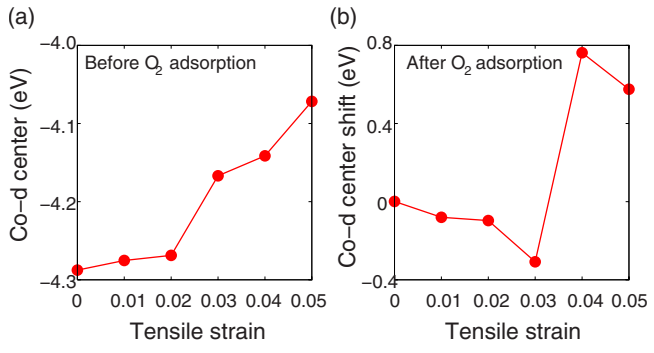

FIG. 7. (Color online) (a) The surface Co d-band center before O_2 adsorption. (b) The shift of surface Co d-band center from the bare to the O_2-adsorbed state, relative to the zero strain condition.

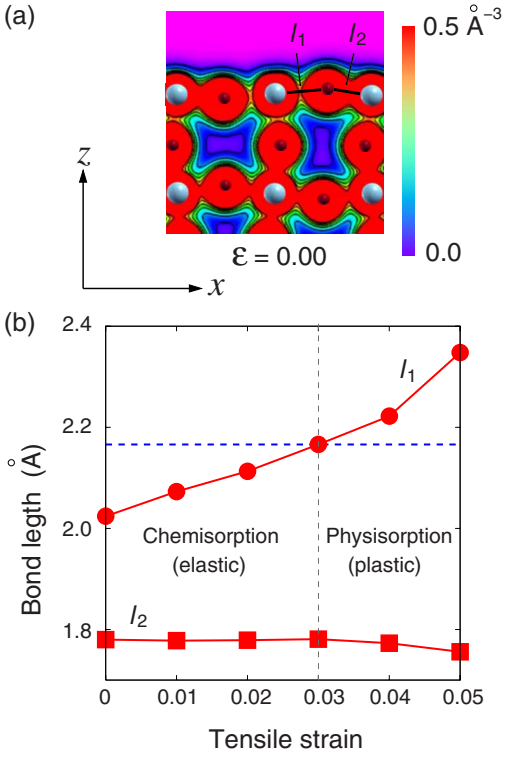

FIG. 8. (Color online) (a) Charge-density distribution of the valance electrons on the LCO film cross section CoO_2 xz plane at zero strain, and (b) the Co-O bond lengths l_1 (circles) and l_2 (squares) as a function of strain. Dashed horizontal line indicates, as a bond breaking criterion on the surface, the maximum Co-O bond length (2.16 Å) before the local relaxation took place in the bulk LCO model at $\varepsilon=0.11$.

negative for $\varepsilon \leq 0.03$. The relative increase in the magnitude of this downshift for $\varepsilon \leq 0.03$ means that the system energy reduces by a larger amount upon oxygen chemisorption when strained, and thus, favors "stronger" chemisorption with lower E_{ad}. From $\varepsilon=0.03$ to $\varepsilon=0.04$, the Co d-band center further increases on the $LaCoO_3$ surface without an adsorbed O_2 molecule. On the other hand, the shift of the Co d-band center on the $LaCoO_3$ surface with the adsorbed O_2 molecule becomes strongly positive at $\varepsilon=0.04$. This suggests that the O_2 adsorbed state becomes relatively less stable, and thus the increase in E_{ad} beyond $\varepsilon=0.03$. Furthermore, at $\varepsilon \geq 0.04$, we observe stark differences in the local Co d- and O p-orbital DOS. When $\varepsilon \geq 0.04$, two separate peaks of the O p orbital remains with only a small overlap with the Co d orbital [Fig. 6(b) for $\varepsilon=0.04$] and does not modify the Co d-band DOS noticeably. This indicates that the oxygen adsorption mechanism changes from chemisorption to physisorption. As a result, the Co d-band shift becomes larger at higher strain, making O_2 adsorption less stable [Figs. 5 and 7(b)]. This transition coincides with the local relaxations beyond $\varepsilon=0.03$. This elastoplastic configuration change is illustrated in Fig. 8. The surface has nonuniform bond lengths even at $\varepsilon=0$. The longer bond l_1 increases while l_2 stays nearly constant up to $\varepsilon=0.03$. Contracting of l_2 along with faster elongation of l_1 for $\varepsilon>0.03$ signifies that the longer bond l_1 was broken. At this point, l_1 reaches the maximum bond length [dashed horizontal line in Fig. 8(b)]

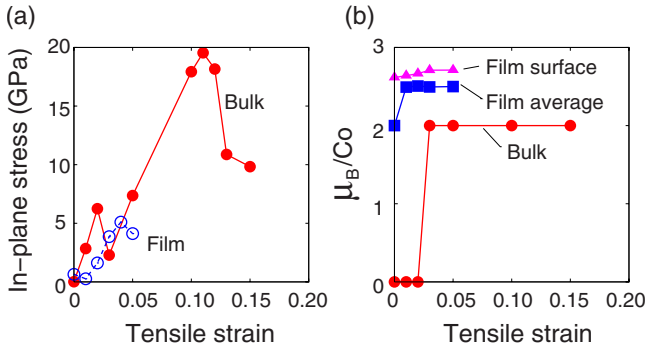

FIG. 9. (Color online) (a) In-plane stress as a function of tensile strain of the bulk (filled circles) and the film (open circles) $LaCoO_3$ models. (b) Change in magnetization under strain for the bulk (circles), film average (squares), and film surface (triangles).

of 2.16 Å. This bond length corresponds to the value incipient to the local relaxation in the bulk LCO model at $\varepsilon=0.11$, and this criterion also supports the breaking of the Co-O l_1 bond on the surface. Consequently, the surface Co can bind more strongly to some of its neighboring O atoms, and therefore could not provide its electrons to hybridize appreciably with the adsorbing oxygen molecule. Once again, from $\varepsilon=0.04$ to $\varepsilon=0.05$ increasing the strain facilitates adsorption as reflected in the decrease in E_{ad} but now in the physisorption mode.

IV. CONCLUSION

The capacity of the material to sustain the stress imposed by the strain state is the critical factor that influences the Co-O bonding to either favor or disfavor the energetics discussed in this work. Figure 9(a) shows the strain states at which the stress drops in the bulk and in the film, when a spin-state transition takes place or when there are local relaxations. The spin-state transitions are shown in Fig. 9(b); they coincide well with the stress relaxations from 0.62 to 0.32 GPa at $\varepsilon=0.01$ for the film, and from 6.3 to 2.3 GPa at $\varepsilon=0.03$ in the bulk $LaCoO_3$ models. There is no spin-state transition on the surface of the $LaCoO_3$ film model. The magnetoelastic transition in the bulk correlated well with the significant increase in E_{vac}^{B} shown in Fig. 2. The decrease in the stress at higher strains, specifically around $\varepsilon=0.13$ for the bulk model and $\varepsilon=0.04$ for the film model corresponds to the Co-O bond breaking and reforming during local relaxations. This elastoplastic transition governed the increase in the $E_{vac}^{S,B}$ and E_{ad}. The local stress relaxations take place at very large strains for this ideal defect-free bulk LCO model. Structural disorder due to point defects or extended defects would allow such relaxations to take place at lower strains.

In conclusion, we provided a detailed microscopic description of the mechanisms by which strain influences oxygen-vacancy formation as well as oxygen adsorption on $LaCoO_3$. Three competing mechanisms were identified. Elastic stretching of the Co-O bond decreases the $E_{vac}^{B,S}$ and E_{ad}. Local relaxations at high strain states create stronger Co-O bonds, trapping the lattice oxygen with higher $E_{vac}^{B,S}$ and disfavoring chemisorption with higher E_{ad}. Spin-state transition from LS to IS strengthens the Co-O bonds and increases E_{vac}^{B}. In particular, we discovered the competition of the magnetoelastic versus elastoplastic effects on oxygen-vacancy formation, and the change in the O_2 adsorption mechanism from chemisorption to physisorption at large strains. Our results illustrate the exciting potential of modulating the reactivity by controlling the strain state of $LaCoO_3$, related perovskite oxides and other ionic materials that exhibit strain-driven transitions in magnetic or electronic structure. Beyond uniform planar strain in thin films, the strain fields around the dislocations[32] can also be considered for modulating the reactivity of such oxide systems. The insights obtained here are also important for motivating experimental and theoretical work to separate out the indirect chemical effects of strain from its direct effects on the magnetic state transitions.

ACKNOWLEDGMENTS

The authors acknowledge the U.S.-DOE, Basic Energy Sciences, Grant No. DE-SC0002633 for financial support, and the National Science Foundation for computational support through the TeraGrid Advanced Support Program, Grant No. TG-ASC090058.

*Corresponding author; byildiz@mit.edu

[1] Y. Ding, D. Haskel, Y.-C. Tseng, E. Kaneshita, M. van Veenendaal, J. F. Mitchell, S. V. Sinogeikin, V. Prakapenka, and H. K. Mao, Phys. Rev. Lett. **102**, 237201 (2009).
[2] A. D. Rata, A. Herklotz, K. Nenkov, L. Schultz, and K. Dörr, Phys. Rev. Lett. **100**, 076401 (2008).
[3] S. Xu, Y. Moritomo, K. Mori, T. Kamiyama, T. Saito, and A. Nakamura, J. Phys. Soc. Jpn. **70**, 3296 (2001).
[4] J. M. Rondinelli and N. A. Spaldin, Phys. Rev. B **79**, 054409 (2009).
[5] P. G. Radaelli and S. W. Cheong, Phys. Rev. B **66**, 094408 (2002).
[6] S. B. Adler, Chem. Rev. **104**, 4791 (2004).
[7] E. A. Kotomin, Phys. Chem. Chem. Phys. **10**, 4644 (2008).
[8] Y. L. Lee, J. Kleis, J. Rossmeisl, and D. Morgan, Phys. Rev. B **80**, 224101 (2009).
[9] M. S. D. Read, M. S. Islam, G. W. Watson, F. King, and F. E. Hancock, J. Mater. Chem. **10**, 2298 (2000).
[10] C. Castellarin-Cudia, S. Surnev, G. Schneider, R. Podlucky, M. G. Ramsey, and F. P. Netzer, Surf. Sci. **554**, L120 (2004).
[11] D. O. Klenov, M. Donner, B. Foran, and S. Stemmer, Appl. Phys. Lett. **82**, 3427 (2003).
[12] D. J. Shu, S. T. Ge, M. Wang, and N. B. Ming, Phys. Rev. Lett. **101**, 116102 (2008).
[13] M. Mavrikakis, B. Hammer, and J. K. Nørskov, Phys. Rev. Lett. **81**, 2819 (1998).
[14] J. B. Goodenough and J. Zhou, Chem. Mater. **10**, 2980 (1998).
[15] N. Sata, K. Eberman, K. Eberl, and J. Maier, Nature (London)

408, 946 (2000).
[16] A. J. Jacobson, Chem. Mater. **22**, 660 (2010).
[17] J. Garcia-Barriocanal, A. Rivera-Calzada, M. Varela, Z. Sefrioui, E. Iborra, C. Leon, S. J. Pennycook, and J. Santamaria, Science **321**, 676 (2008).
[18] A. Kushima and B. Yildiz, J. Mater. Chem. **20**, 4809 (2010).
[19] T. J. Pennycook, M. J. Beck, K. Varga, M. Varela, S. J. Pennycook, and S. T. Pantelides, Phys. Rev. Lett. **104**, 115901 (2010).
[20] M. Sase, K. Yashiro, K. Sato, J. Mizusaki, T. Kawada, N. Sakai, K. Yamaji, T. Horita, and H. Yokokawa, Solid State Ionics **178**, 1843 (2008).
[21] K. Dörr, O. Bilani-Zeneli, A. Herklotz, A. D. Rata, K. Boldyreva, J.-W. Kim, M. C. Dekker, K. Nenkov, L. Schultz, and M. Reibold, Eur. Phys. J. B **71**, 361 (2009).
[22] J. P. Perdew, J. A. Chevary, S. H. Vosko, K. A. Jackson, M. R. Pederson, D. J. Singh, and C. Fiolhais, Phys. Rev. B **46**, 6671 (1992).
[23] V. I. Anisimov, J. Zaanen, and O. K. Andersen, Phys. Rev. B **44**, 943 (1991); V. I. Anisimov, F. Arysasetiawan, and A. I. Lichtenstein, J. Phys.: Condens. Matter **9**, 767 (1997).
[24] L. Wang, T. Maxisch, and G. Ceder, Phys. Rev. B **73**, 195107 (2006).
[25] G. Kresse and D. Joubert, Phys. Rev. B **59**, 1758 (1999); P. E. Blöchl, *ibid.* **50**, 17953 (1994).
[26] G. Kresse and J. Hafner, Phys. Rev. B **47**, 558 (1993); G. Kresse and J. Furthmüller, *ibid.* **54**, 11169 (1996).
[27] H. J. Monkhorst and J. D. Pack, Phys. Rev. B **13**, 5188 (1976).
[28] D. Fuchs, E. Arac, C. Pinta, S. Schuppler, R. Schneider, and H. v. Löhneysen, Phys. Rev. B **77**, 014434 (2008).
[29] D. A. Andersson, S. I. Simak, N. V. Skorodumova, I. A. Abrikosov, and B. Johansson, Proc. Natl. Acad. Sci. U.S.A. **103**, 3518 (2006).
[30] H. Hsu, K. Umemoto, M. Cococcioni, and R. Wentzcovitch, Phys. Rev. B **79**, 125124 (2009).
[31] T. A. Baker, C. M. Friend, and E. Kaxiras, J. Phys. Chem. C **113**, 3232 (2009).
[32] J. Wintterlin, T. Zambelli, J. Trost, J. Greeley, and M. Mavrikakis, Angewandte Chemie **42**, 2850 (2003).